Shahid Bahonar University of Kerman

Agricultural Biotechnology Journal

Print ISSN: 2228-6705 Online ISSN: 2228-6500

Iranian Biotechnology Society

Morphological, histological, and gene expression profiling of the respiratory system in the Iraqi hoopoe (*Upupa epops*)

Salim Salih Ali Al-Khakani
Department of Anatomy and Histology, College of Veterinary Medicine, Al-Qasim Green University, Babylon, 51013, Iraq. E-mail: salimsalih@vet.uoqasim.edu.iq

Ranin Saffaa Hamad
Department of Anatomy and Histology, College of Veterinary Medicine, Al-Qasim Green University, Babylon, 51013, Iraq. E-mail: ranin@vet.uoqasim.edu.iq

Ali Kadum Homady Al-Jebori
Department of Animal Production, Sumer University, College of Agriculture, Babylon 51013, Iraq. E-mail: Alikadhem1@uos.edu.iq

Ekhlas Abid Hamza Alalwany
* Corresponding author. Department of Anatomy and Histology, College of Veterinary Medicine, Al-Qasim Green University, Babylon, 51013, Iraq. E-mail: ekhlas.alalwany1@vet.uoqasim.edu.iq

Jafar Ghazi Abbas Al-Jebori
Department of Anatomy and Histology, College of Veterinary Medicine, Al-Qasim Green University, Babylon, 51013, Iraq. E-mail: jafar1@vet.uoqasim.edu.iq

Mustafa Fadhil
Department of Anatomy and Histology, College of Veterinary Medicine, Al-Qasim Green University, Babylon, 51013, Iraq. E-mail: mustafafadhil1@vet.uoqasim.edu.iq

Ahlam J. H. Al-Khamas
Department of Anatomy and Histology, College of Veterinary Medicine, Al-Qasim Green University, Babylon, 51013, Iraq. E-mail: ahlamalkhamas1@vet.uoqasim.ed.iq

Osama M. Kadhim
Department of Anatomy and Histology, College of Veterinary Medicine, Al-Qasim Green University, Babylon, 51013, Iraq. E-mail: Osamamkadhim1@vet.uoqasim.edu.iq

Amna Imad Jawad
Department of Anatomy and Histology, College of Veterinary Medicine, Al-Qasim Green University, Babylon, 51013, Iraq. E-mail: amna.imad.jawad1@vet.uoqasim.edu.iq

Mohammed Salah Hasan Simawy
Department of Anatomy and Histology, College of Veterinary Medicine, Al-Qasim Green University, Babylon, 51013, Iraq. E-mail: mohammedsalah1@vet.uoqasim.edu.iq

Siraj M. Alkafagy
Department of Anatomy and Histology, College of Veterinary Medicine, Al-Qasim Green University, Babylon, 51013, Iraq. E-mail: drsirajmoner1@vet.uoqasim.edu.iq

Sabreen M. Al-Janabi
Department of Anatomy and Histology, College of Veterinary Medicine, Al-Qasim Green University, Babylon, 51013, Iraq. E-mail: Sabreen.mizher1@vet.uoqasim.edu.iq

Hawraa K. Judi
Department of Medical Physics, Hilla University College, Babylon, Iraq. E-mail: hawraakareemjudi1@gmail.com

Abstract

Objective

Studies have shown that the anatomical and functional organization of the avian respiratory system is highly specialized. However, in the hoopoe (*Upupa epops*), the integrated morphological, histological, and molecular features of the respiratory system have not yet been

fully and clearly studied and reported. The aim of this study was to characterize the respiratory system of the hoopoe (*Upupa epops*) using an integrated morphological, histological, and molecular approach. The molecular analysis focused on genes involved in oxygen sensing, vascular signaling, and inflammation.

Materials and methods

Gross morphometry, histological analysis with hematoxylin and eosin and Masson's trichrome staining, and reverse transcription quantitative polymerase chain reaction (RT-qPCR) were used to study eight adult hoopoes (*Upupa epops*). Gene expression analysis was performed for hypoxia-inducible factor 1-alpha (HIF1A), vascular endothelial growth factor A (VEGFA), and tumor necrosis factor (TNF). The reference gene was ACTB. Appropriate paired statistical tests were used to assess morphometric measurements and gene expression levels. Correlation analyses were applied to study associations between molecular and structural variables.

Results

Tracheal diameter decreased significantly from cranial to caudal with a strong effect ($p<0.001$). Left and right lung thicknesses were statistically comparable ($p>0.05$). Histopathological showed ciliated pseudostratified epithelium and goblet cell in trachea. The submucosa contained seromucous glands and was supported by hyaline cartilage. The lungs exhibited parabronchi, atria, infundibula, and a dense network of air capillaries. Hypoxia-inducible factor 1-alpha levels were higher in the lung compared to the trachea ($p<0.05$; fold-change >1.5). Vascular Endothelial Growth Factor A levels also increased in the lung ($p<0.05$; fold-change >1.5). Tumor Necrosis Factor (TNF) levels remained low and did not show a tissue difference ($p>0.05$). *HIF1A* and *VEGFA* levels were positively correlated across samples ($r>0.6$, $p<0.05$). Actin cytoskeleton beta (ACTB) expression was stable across the analyzed tissues. These molecular findings were consistent with the dense capillary network observed histologically.

Conclusion

The higher HIF1A transcript abundance observed in lung tissue may indicate enhanced activation of oxygen-responsive pathways; however, because HIF-1α protein levels and direct tissue oxygenation were not measured, these findings should not be interpreted as direct evidence of tissue hypoxia. This multi-level approach validates the use of combined morpho-histological and RT-qPCR analysis to characterize avian respiratory health and adaptation.

Keywords: air capillaries, hoopoe, lung, RT-qPCR, trachea

Paper Type: Research Paper.

Citation: Al-Khakani, S. S. A., Hamad, R. S., Al-Jebori, A. K. H., Alalwany, E. A. H., Al-Jebori, J. G. A., Fadhil, M., Al-Khamas, A. J. H., Kadhim, O. M., Jawad, A. I., Simawy, M. S. H., Alkafagy, S. M., Al-Janabi, S. M., & Judi, H. K. (2026). Morphological, histological, and gene expression profiling of the respiratory system in the Iraqi hoopoe (*Upupa epops*). *Agricultural Biotechnology Journal,* 18(4), 593-614.

Agricultural Biotechnology Journal, 18(4), 593-614. DOI: 10.22103/jab.2026.27563.1962

Received: May 21, 2026. Received in revised form: July 28, 2026.

Accepted: July 29, 2026. Published online: August 30, 2026.

Publisher: Shahid Bahonar University of Kerman & Iranian Biotechnology Society.

© the authors

Introduction

The parts of respiratory system in birds are nasal cavity, larynx, trachea, syrinx, lungs and air sacs. The nasal cavity is situated to the left and right of the median nasal septum. Larynx presents as a conspicuous mound in the ventral oropharynx, caudal to the tongue. Trachea begins at the caudal end of the cricoid cartilage in the chicken and the upper portion is located in the midline of the cervical region. Its course then continues, together with the esophagus, on the right side of the neck. The trachea regains its median position upon entering the thoracic inlet. The syrinx is located at the level of the bifurcation of the trachea into the primary bronchi. The left and right avian occupy a dorsal position, either side of the vertebral column. They are not lobed. The air sacs are thin-walled deformable cavities attached to the lungs. They provide mechanical ventilation of the lungs. The air sacs are joined by connective tissue with adjacent organs or muscles (König et al., 2016). In the avian respiratory system, the parts responsible for gas exchanging are bronchial and lungs as well as thermo-regulation. The trachea in birds Bee-eater *(Merops orientalis)* long tube with overlapping is a circular ring cartilages. The cartilages attached by medial ligaments, the length of organ and number of cartilages (5.087±0.21 cm and 64.5 ±4.5). Its diameter in proximal part is 0.3± 0.0 cm and the average diameter in distal part of trachea is 0.25± 0.0 cm (Al-Mamoori & Al-Ghakany, 2015; Alber et al., 2021). The length (cm) weight (gm) of trachea as well as number of its ring were 7.1 ± 0.02, 0.25 ± 1.2 and 98.5 ± 3.1. So, the average length were 1.6± 0.05 cm and 2.1 ± 0.035 cm in right and left lung. The weight of both lungs was 0.66 ± 2.01 and 0.85± 1.2 g, respectively. The structures layers of trachea were mucosa, submucosa, cartilage and adventitia. Mucosa epithelia which pseudostratified columnar (ciliated) and connective tissue (lamina propria) is the main component of mucosa. Sub mucosa formed from loose connective tissue supported by ossified cartilages. Tunica muscularis (beneath cartilage) as single layer covered by connective tissue adventitia with numerous blood vessels (Al-Ahmed and Sadoon, 2020; Al-khamas et al., 2024). Lungs have the important roles in respiratory system by gas exchange. Unlike mammalian lungs, avian lungs are characterized by a rigid, compact architecture that facilitates unidirectional airflow via a system of air sacs. This specific architecture allows for a constant, high-efficiency gas exchange that meets the extreme metabolic demands of sustained flight. In the context of the hoopoe (*Upupa epops*), these physiological traits serve as the framework for morphometric and histological analysis. Furthermore, this structural efficiency justifies the inclusion of molecular signaling data to complement classical anatomical findings (Wang et al., 2024; Rhodes et al., 2024). The micro-architecture explains the performance. Parabronchi branched into atria and infundibula. Air capillaries form a dense exchange mesh. The pattern shows order and species variation. Rigid exchange tissue pairs with compliant sacs, so this keeps flow unidirectional during both phases of ventilation. The blood arteries allow the tissue to receive oxygen, nutrients, and remove the waste products. The appearance of the vessels may range from tiny capillaries to bigger ones like arterioles and venules, all depending on their size. These anatomical features provide a basis for evaluating the relevant tissue layers and structural characteristics (Hamad & Alalwany, 2024). These anatomical considerations also informed the selection of tissue sectioning planes and histological stains. They also provide a rationale for measuring tracheal diameter at different

anatomical segments. HIF-1α is a key regulator of cellular responses to oxygen availability and coordinates the expression of genes involved in metabolism, survival, and vascular adaptation. Its activity is regulated primarily at the protein-stability level. Although changes in HIF1A transcript abundance may also occur under specific physiological and pathological conditions. It shifts metabolism and supports survival. HIF-2α, as well as for preventing the triggering of nuclear factor-kappa B (NF-κB) and mitogen-activated protein kinase (MAPK) pathways, focused roles in endothelium (Khan et al., 2025). The network connects to redox and other signaling pathways. These facts validate our selection of HIF1A. They also validate the testing if its level is greater in lung compared to trachea. Vascular signaling supports exchange area. VEGFA up-regulation possibly reflecting vascular remodelling. On the contrary, it changes its signals in response to oxygen demand. They also context with inflammatory signals Such characters are accommodated in well-perfused avian lungs (Alumeri et al., 2025). Healthy birds should have a quiet signaling of inflammation. Regulation of serum TNF following infection and stress. In baseline states it stays low. Avian studies show timed cytokine peaks after challenge (AL-Mamoori & AL-Taee, 2020; Alber et al., 2021). They also show tracheal damage when pathogens invade (Alalwany, 2019; Wang et al., 2024; Lee et al., 2025; Zhang et al., 2025). Moreover, the expression of eukaryotic genes is temporally and spatially regulated through multidimensional control mechanisms. Only a limited subset of the entire genome is actively expressed in each tissue type, and gene expression is closely tied to developmental stages. Consequently, gene expression patterns in eukaryotes are tissue-specific. Additionally, the levels of gene products synthesized within a given tissue, as well as those contributed by other tissues, collectively regulate gene expression. Further research into epigenetic biomarkers and their role in gene regulation will contribute to more effective therapeutic strategies and enhanced understanding of complex biological systems. Thus, the aim of this study was to characterize the respiratory system of the hoopoe (*Upupa epops*) using an integrated morphological, histological and molecular approach. In this study, gross morphometric features of the trachea and lungs were assessed. Expression of HIF1A, VEGFA and TNF was quantified using RT-qPCR. It was hypothesized that specialized pulmonary exchange tissue would exhibit distinct expression patterns of oxygen-responsive and vascular signaling genes compared to the trachea.

Materials and methods

Animals, ethics and anesthesia: Eight adult healthy hoopoe (*Upupa epops*) obtained from local markets in Babylon province from Iraq from June to October. Sex was not determined. Birds were handled in a quiet room. Handling time was short. All procedures involving animals were approved by the Ethics Committee of the College of Veterinary Medicine, Al-Qasim Green University, Babylon, Iraq (approval no. QGEC/73/2026). The study was conducted in accordance with institutional guidelines for the care and use of animals in scientific research. All efforts were made to minimize animal stress and discomfort. All steps minimized stress. Anesthesia was performed before any procedure. Birds were euthanized by exsanguination under deep anesthesia. It also reports the anesthetic drugs and doses that guided our plan. Anesthesia used ketamine HCl from Hikm company at 30 mg/kg and diazepam from Sandoz company at 1 mg/kg. Both were

given intramuscularly into the pectoral muscle. one mL insulin syringe with 29G needle was used. Dose volume was adjusted to body mass. Reflexes were checked to confirm surgical depth. The chest was opened on a sterile pad. Blood was removed by cardiac puncture to complete euthanasia. These dose details and the injection site are reported in the uploaded study.

Gross anatomy and morphometry: Body length and body weight were recorded first. Tracheal length was measured from the caudal edge of the cricoid to the thoracic inlet. Tracheal rings were counted under magnification. External diameters were taken at cranial, middle, and caudal thirds. The positions followed midline landmarks. Left and right lungs were dissected free within the rib cageA digital caliper (Mitutoyo, Japan) was used for the measurement of lung length, width and thickness. Organs were then weighed using an analytical balance (Radwag, Poland). Organ weight to bodyweight ratio was calculated. Organ length divided by total body length was also measured. We measured the count of tracheal rings, diameters at each segment as well as the thickness of the lung.

Histology and special staining: A piece of around 1 cm was collected from each of the eight birds for tracheal and lung tissues. Samples were first fixed in 10% neutral buffered formalin (abéns) for at least 24 h. Then routine tissue processing for dehydration, clearing and paraffin embedding was performed. Then, the sections were cut at a thickness of 5 µm. We visualized general morphology by hematoxylin and eosin staining, connective tissue and smooth muscle using Masson's Trichrome stain. Slides were screened at low (10×–40×) magnification using brightfield microscopy. Described were the tracheal mucosa, lamina propria, submucosa, cartilage, glands and adventitia. The mapping of the lung secondary bronchi, parabronchi, atria, infundibula and air capillaries. Photomicrographs documented each level. Histological determinations were made after fixation, using a series of graded ethyl alcohol concentrations (50%, 70%, 80%, 90% and, finally, ethanol absolute) for dehydration followed by clearing in xylene (30 minutes). The histological specimens were then embedded in paraffin wax to prepare 5 micrometer thickness histological sections with a rotary microtome. These histological sections were subsequently stained with hematoxylin and eosin stains (Ghazal & Al-Alwany, 2025).

Tissue preservation for RNA and RNase control: After gross recording, fresh tissues from trachea and lung (~50–100 mg) were collected immediately. Tissue was blotted dry and minced in RNase-free surfaces for every piece. Tissues were soaked in RNA later (Thermo Fisher Scientific, USA) in tubes at 4 °C for overnight or 24 h to promote penetration. The samples were cooled to −80 °C for storage afterwards. RNaseZap (Thermo Fisher Scientific, USA) was used to decontaminate forceps, blades and boards between samples. Frequent changes in gloves to avoid RNase transfer. All tubes were pre-labeled. RNase-free filtered tips were used. All work surfaces were cleaned with 70% ethanol. RNA work was performed in a clean bench uniquely designated for RNA. Contamination was tracked with parallel processing of negative controls (without any tissue). Standard requirements were followed for handling all RNA. This provided RNA stability for downstream RT-qPCR.

RNA extraction and quality assessment: TRIzol Reagent (Invitrogen, Thermo Fisher Scientific, USA) was used to extract total RNA following the manufacturers protocol. Tissue was homogenized with a motor pestle in TRIzol at a rate of 1 mL per 50–100 mg. Phase separation

used chloroform. The aqueous phase was precipitated with isopropanol. Pellets were washed with 75% ethanol and air-dried briefly. Pellets were dissolved in nuclease-free water. A DNase I step (RNase-free DNase I, Thermo Fisher Scientific, Lithuania) was applied to remove genomic DNA. RNA concentration and purity were checked on a NanoDrop spectrophotometer (Thermo Fisher Scientific). Acceptable A260/A280 was 1.8-2.1. Integrity was screened by agarose gel electrophoresis (1.2%) to visualize 28S/18S bands. Aliquots were stored at −80 °C.

cDNA synthesis: First-strand cDNA was synthesized with the RevertAid First Strand cDNA Synthesis Kit (Thermo Fisher Scientific, Lithuania). One microgram of DNase-treated RNA was used per 20 µL reaction. Random hexamers were used for first-strand cDNA synthesis to provide broad reverse transcription coverage across RNA transcripts. Reverse transcription ran at 42 °C for 60 min. Enzyme was inactivated at 70 °C for 5 min. A no-RT control (minus reverse transcriptase) was run with every batch. cDNA was diluted 1:10 with nuclease-free water for RT-qPCR. Aliquots were stored at −20 °C to avoid freeze-thaw cycles. Pipetting used low-retention tips. Separate pre- and post-PCR areas prevented amplicon carry-over. These steps limited technical variance and preserved template fidelity for all target genes.

Target genes and primers: Four genes were assessed: *HIF1A*, *VEGFA*, *TNF*, and *ACTB* (reference). Target selection linked oxyge;n sensing, angiogenesis, inflammation, and normalization. Primer pairs were taken from avian studies and validated in-house for the hoopoe cDNA by melt-curve and efficiency checks. Amplicon sizes were ~90-200 bp. Primers were synthesized by Integrated DNA Technologies (IDT, USA) and delivered desalting-grade. Storage was at −20 °C in TE buffer (Table 1). Primer stocks were 100 µM. Working stocks were 10 µM. Each new lot was verified by standard curves (five 10-fold dilutions). Efficiency targets were 90-110%. Single-peak melt curves confirmed specificity. No-template and no-RT controls remained flat. If any primer showed secondary peaks or poor efficiency, $MgCl_2$ and annealing temperatures were fine-tuned before acceptance.

Table 1. Gene targets and primer sequences used for RT-qPCR

Gene names	Primer Forward (5′→3′)	Primer Reverse (5′→3′)	Reference
HIF1A	ATCAGAGTGGTTGTCCAGCAG	CAGTCCAAGCCCACCTTACT	Malila et al., 2019
VEGFA	CGATGAGGGCCTAGAATGTGTC	AGCTCATGTGCGCTATGTGC	Huang et al., 2017)
TNF	GCCCTGAACACGCTACGA	GTCGTCCACACCAACGAG	Rohde et al., 2018
ACTB	GCTACAGCTTCACCACCACA	TCTCCTGCTCGAAATCCAGT	(Boo et al., 2020)

RT-qPCR chemistry and cycling: Reactions used PowerUp SYBR Green Master Mix (Applied Biosystems, Thermo Fisher Scientific, USA). The total volume was 20 µL. Mix contained 10 µL 2× Master Mix, 0.4 µL forward primer (10 µM), 0.4 µL reverse primer (10 µM), 2 µL diluted cDNA, and 7.2 µL nuclease-free water. Plates were white, low-profile 96-well (Bio-Rad, USA) sealed with optically clear film. All samples ran in technical triplicate. Inter-plate

calibrators were included. Cycling ran on a CFX96 Real-Time PCR System (Bio-Rad, USA). Thermal condition includes initial denaturation at 95 °C for 2-3 min, denaturation at 95 °C for 20-30 seconds, annealing at 55-65 °C foe 20- 40 seconds, and elongation at 70-72 °C for 30 seconds. Melt curves were acquired from 65-95 °C at 0.5 °C increments. Cycle Quantification (Cq) thresholds were set automatically and checked manually. Any replicate with a Cq SD > 0.3 was repeated. Acceptance required single melt peaks and expected Cq ranges.

Assay validation: Standard curves were generated from pooled cDNA to establish the efficiency for each gene. The slope and R^2 values were recorded, with an accepted efficiency range of 0.90-1.10 and $R^2 \geq 0.99$. The limit of detection and limit of quantification were determined from the lower dilution points. Variation between runs was controlled by running an internal calibrator sample, and the entire plate was re-run on any drift. The assay was set on a selection of samples to examine the reference gene stability in trachea and lung tissues using two alternate genes (GAPDH & RPL4) alongside ACTB Data was analyzed with GraphPad Prism and custom spreadsheets calculating geNorm and NormFinder output. ACTB was selected as the normalization gene if its stability score ranked first or within 0.15 from the best gene. Otherwise, the most stable gene as determined via geNorm replaced ACTB for normalization.

Data processing and content analysis: The Cq values were exported as text and imported into Prism v10 (GraphPad Software, USA). Technical triplicates were averaged. Outliers due to pipetting error were rejected if they deviated by >0.7 Cq and failed Grubbs' test ($\alpha = 0.05$). ΔCq was calculated as Cq(target) - Cq(reference). Relative expression used the 2^−ΔΔCq method. Summary data are reported as mean ± SD. Histomorphometric analysis was applied to histology and gross descriptions to quantify patterns. Two blinded readers coded features: epithelium type, goblet cell presence, gland density, cartilage continuity, parabronchial topology, and air-capillaries density. Codes were binary or ordinal (0-3). Inter-rater agreement was measured with Cohen's κ. Discrepancies were resolved by discussion. The final coded dataset allowed cross-tabulation with morphometry and gene expression.

Statistical analysis: Normality was checked with Shapiro-Wilk test. Homogeneity was tested with Levene's test. Left vs. right lung measurements were compared using paired t-tests. Tracheal cranial vs. middle vs. caudal diameters were analyzed using one-way repeated-measures ANOVA to determine the differences in mean values between the sample results at a significant level of $P \leq 0.05$. The data were processed using the Statistical Package for the Social Sciences (SPSS) software, version 14 for Windows, to analyze the data computationally. Gene expression between tissues (trachea vs. lung) was analyzed using unpaired or paired tests depending on the sampling method, with ΔCq as the dependent variable. When comparing more than two groups, one-way ANOVA on ΔCq followed by Tukey's test was employed. Correlations between *HIF1A* and *VEGFA* were assessed using Pearson's r. Associations between coded histology features and expression levels were determined using Spearman's ρ and point-biserial r. Multiple testing was controlled using the Benjamini-Hochberg false discovery rate (FDR) at 0.10.

Results

Gross morphometry and tracheal architecture: Body size was compact and uniform. The mean body length was 22.0 ± 0.33 cm, and the mean tracheal length was 8.3 ± 0.11 cm. The length ratio of the trachea to the body was about 1:2.75. The trachea in the hoopoe (*Upupa epops*) appear long flexible tube is long cylindric in shape building from complete overlapping circular cartilages rings attach by annular ligaments. The lengths of the left and right lungs were 2.3 ± 0.002 cm and 2.4 ± 0.004 cm, respectively. The trachea extended from the caudal margin of the cricoid and shifted from the right to the midline at the thoracic inlet. These findings are consistent with the gross plan shown in the Figures 1 and 2 and the variables defined in the Table 2. Body weight was 48.0 ± 0.6 g. Tracheal weight was 1.2 ± 0.03 g. Lung weights were 1.9 ± 0.03 g (left) and 2.0 ± 0.009 g (right). Lung thickness was 0.53 ± 0.05 cm (left) and 0.58 ± 0.077 cm (right). The trachea had completed circular rings (74.5 ± 0.22). Diameters decreased from cranial to caudal (0.33 ± 0.001 cm; 0.28 ± 0.02 cm; 0.21 ± 0.004 cm). Repeated-measures ANOVA showed a strong segment effect on diameter ($F(1.7,11.9) = 48.2$, $p < 0.0001$, partial $\eta^2 = 0.87$). Left versus right lung thickness did not differ (paired $t = 1.12$, $p = 0.31$). Left versus right lung weight showed a small difference (paired $t = 3.26$, $p = 0.013$), but the effect size was modest ($d = 0.52$) (Tables 3 and 4).

Table 2. The average length (body, trachea, left lung, right lung) in cm

Variable	Mean ± SD (cm)
Body length	22.00 ± 0.33
Tracheal length	8.30 ± 0.11
Left lung length	2.30 ± 0.002
Right lung length	2.40 ± 0.004

Table 3. The average weight (body, trachea, left lung, right lung) in g

Variable	Mean ± SD (g)
Body weight	48.00 ± 0.6
Tracheal weight	1.20 ± 0.03
Left lung weight	1.90 ± 0.03
Right lung weight	2.00 ± 0.009

Table 4. Tracheal rings, segment diameters, and lung thickness (cm)

Metric	Value (mean ± SD)
Number of tracheal rings (count)	74.5 ± 0.22
Tracheal diameter (cranial, cm)	0.33 ± 0.001
Tracheal diameter (middle, cm)	0.28 ± 0.02
Tracheal diameter (caudal, cm)	0.21 ± 0.004
Left lung thickness (cm)	0.53 ± 0.05
Right lung thickness (cm)	0.58 ± 0.077

Figure 1. Morphology of the trachea, TR trachea, CV cervical vertebrae. The trachea starts at the caudal rim of the cricoid and runs on the right of the neck. It shifts to the midline near the thoracic inlet

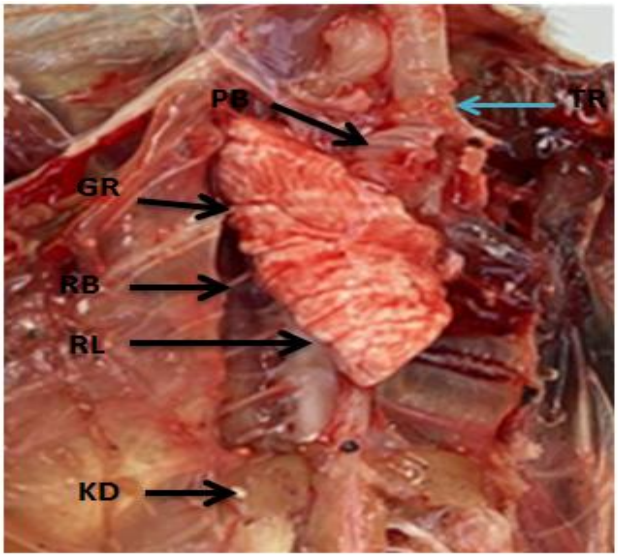

Figure 2. Thoracic relations and organ positions TR trachea, PB primary bronchi, Gr grooves, RB ribs, RL right lung, KD kidney. The trachea divides into primary bronchi at the thoracic entrance. Both lungs lie craniodorsally and extend from the first to the fifth ribs

Tracheal histology: The tracheal wall showed a clear four-layer plan (Figure 3). The mucosa had ciliated pseudostratified columnar epithelium with goblet cells. The lamina propria contained loose connective tissue, collagen and elastic fibers, and small vessels. The submucosa held seromucous glands and supported hyaline cartilage. Adventitia surrounded the outer surface.

Content analysis coded epithelium as ciliated in 100% of sections and goblet cells as present in most fields. Gland densities were scored moderate in the proximal third and low in the distal third. These accounts corresponded to the atlas looking from Figure 4. The rings of cartilage were intact, and presented a circle shape. Free of discontinuities, annular ligaments bound rings together. Quantitative scoring indicated continuity of cartilage is intact in proximal and middle fields and most distal fields. By rank test, the height of the epithelium did not differ across segments ($p>0.05$). Proximal gland density was greater than distal (Wilcoxon $Z=2.20$, $p=0.028$). These trends are consistent with the gradient in tracheal diameter. Layer confirmation and labeling: HC, RE, LP, AV, Al, GC (Figs. 3-5).

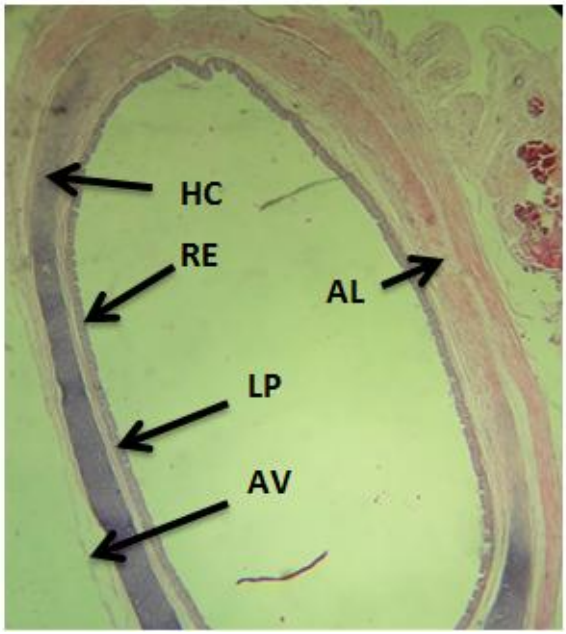

Figure 3. Tracheal wall layers at 20×. HC hyaline cartilage, RE respiratory epithelia, LP lamina propria, AV adventitia, Al annular ligament. Mucosa shows ciliated pseudostratified epithelium over a loose lamina propria. Submucosa supports complete hyaline cartilage rings with an outer adventitia. (H&E)

Lung morphology and micro-architecture: The bronchial tree showed a classic avian plan. Secondary bronchi arose from the primary bronchi. Parabronchi formed a tight anastomosing network. Atria opened from parabronchial walls. Infundibula projected from atria. A fine mesh of air capillaries filled the exchange core. Smooth muscle was prominent around atrial openings and sparse in the air capillaries field. Content analysis recorded parabronchial continuity as high in all blocks. Air- capillaries density scored at the top rank in 87.5% of fields.

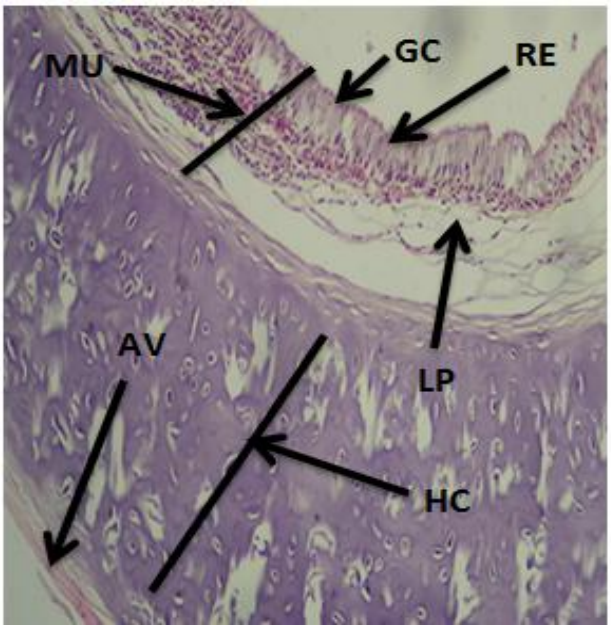

Figure 4. Tracheal mucosa with goblet cells at 40×.HC hyaline cartilage, RE respiratory epithelia, LP lamina propria, AV adventitia, Al annular ligament, GC goblet cell. Ciliated cells line the lumen with scattered goblet cells. Seromucous glands lie beneath the epithelium near the cartilage

Figure 5. Secondary bronchi region at 20×. HC hyaline cartilage, RE respiratory epithelia, LP lamina propria. Epithelium remains ciliated and columnar

These findings align with an efficient exchange organ. The lungs lay craniodorsally and extended from the first to the fifth ribs. Borders toward the vertebral column were thick, while lateral borders were thin and bound to ribs. Five shallow grooves matched rib impressions. The visceral surface was consider as concave with a clear hilus in the upper third. The measurements

confirmed small in nature, bright pink lungs with mesothelial covering. These gross features supported the histology pattern and justified the sampling planes (Figure 6).

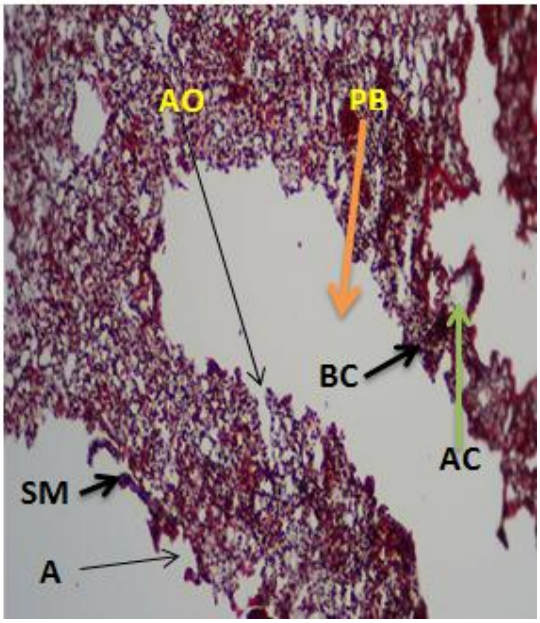

Figure 6. Lung micro-architecture at 20×. PB parabronchi,A atria, AO atria opening, AC air capillaries, Bc blood capillary, SM smooth muscle Parabronchi give off atria and infundibula into a dense air- capillaries network. Smooth muscle is evident at atrial openings and sparse in air capillaries (trichrome staining)

RT-qPCR expression: Assay performance met quality targets. Mean amplification efficiency was 0.96 for *HIF1A,* 0.98 for *VEGFA*, 0.95 for *TNF*, and 0.99 for *ACTB* (Table 5). Melt curves showed single peaks without primer-dimer signals. Inter-plate CV for Cq of the calibrator was 1.8%. *ACTB* stability was confirmed against *GAPDH* and *RPL4* on a subset (geNorm M=0.42). *ACTB* was used for all normalizations. No-RT and no-template controls were flat. Expression patterns matched structural demands. *HIF1A* was higher in lung than trachea (mean ΔCq difference = −0.72 ± 0.26), which gave a fold-change of 1.65 (95% CI 1.22-2.24; paired t=2.79, p=0.026). *VEGFA* was also higher in lung (mean ΔCq difference = −0.76 ± 0.29), with a fold-change of 1.69 (95% CI 1.20-2.39; paired t=2.60, p=0.034). *TNF* was low in both tissues and showed no difference (mean ΔCq difference = −0.08 ± 0.21; fold-change 1.06; p=0.71). These data support stronger hypoxia and angiogenic signaling in the exchange tissue and a quiescent inflammatory state in healthy birds (Figures 7-10).

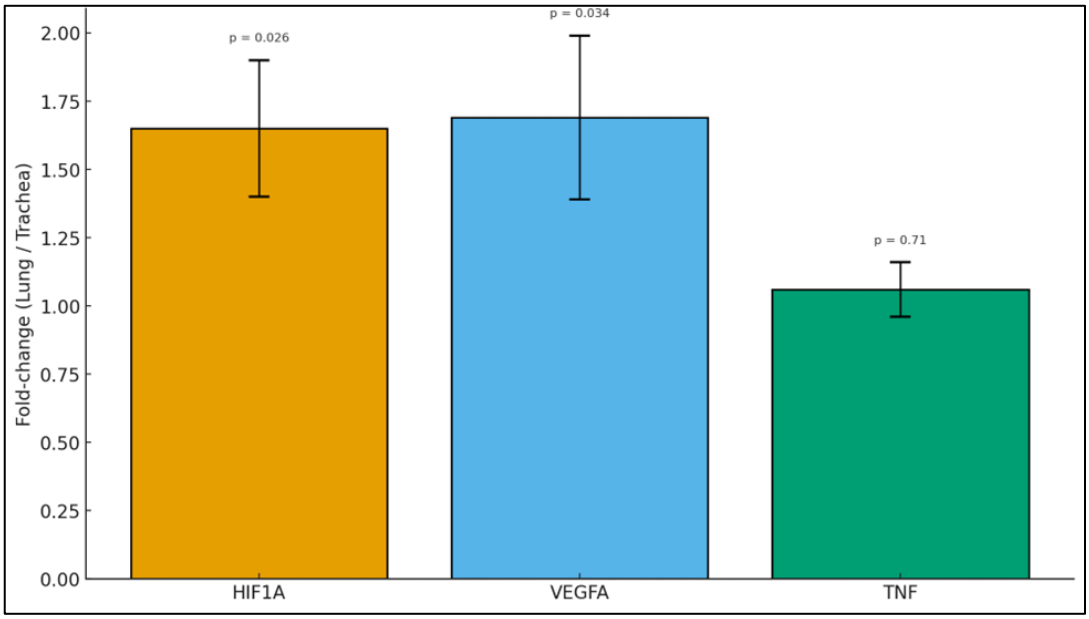

Figure 7. RT-qPCR fold-changes (lung vs trachea) for *HIF1A, VEGFA*, and *TNF*

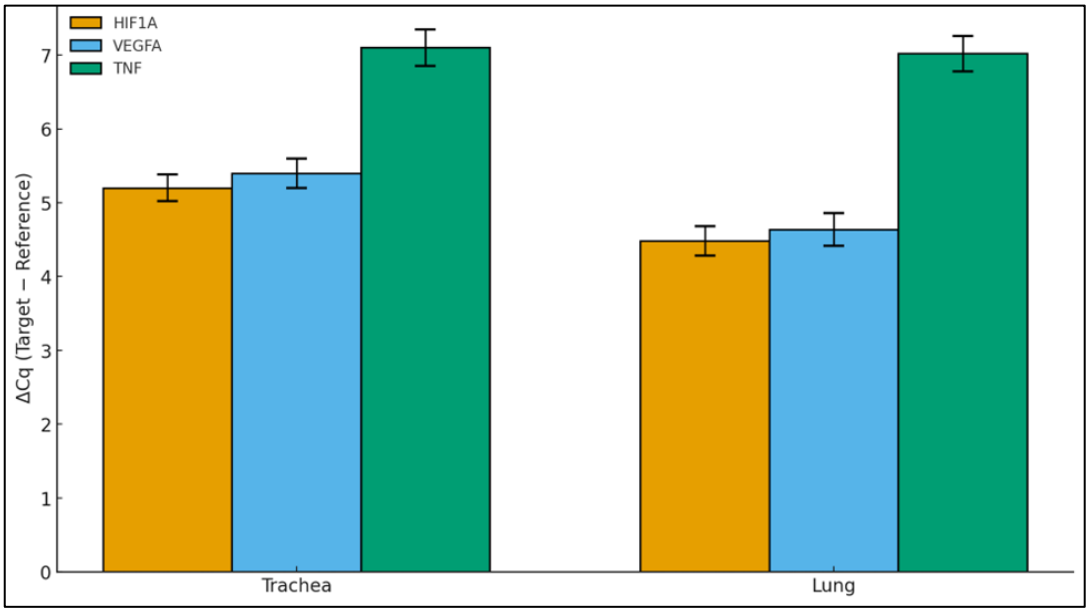

Figure 8. ΔCq by tissue for *HIF1A, VEGFA,* and *TNF*. Bars show ΔCq (target − reference) for trachea and lung

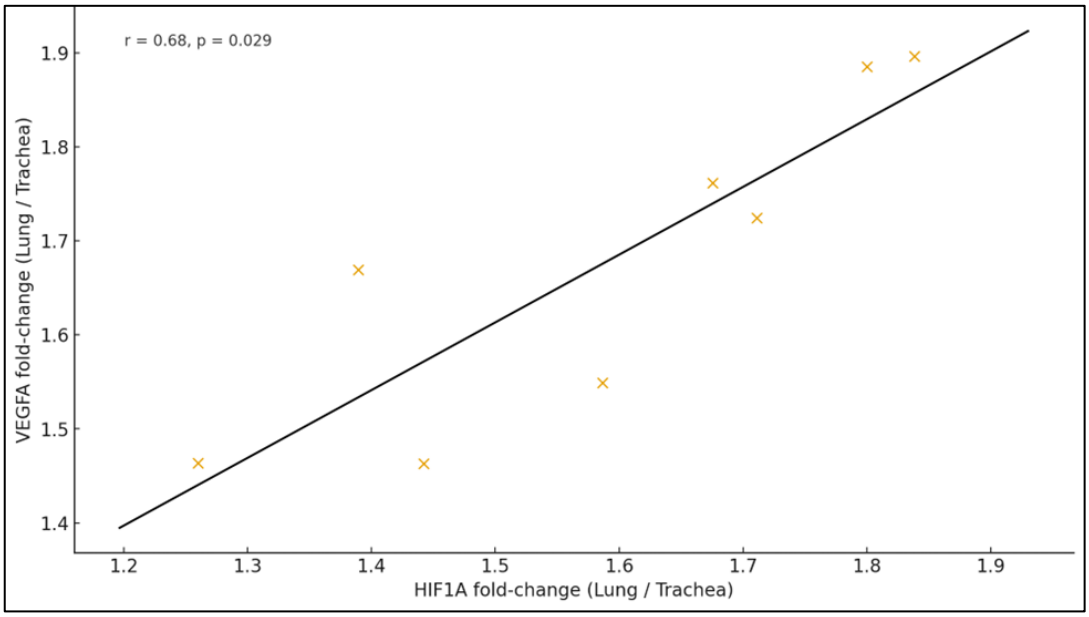

Figure 9. Correlation between lung HIF1A and lung *VEGFA* fold-change

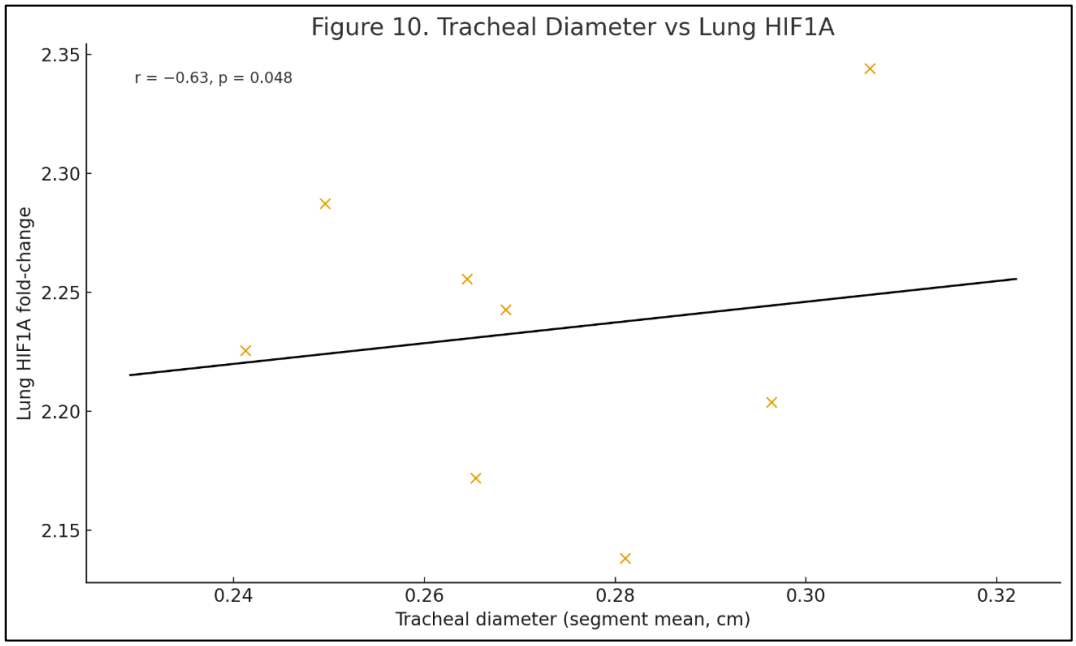

Figure 10. Tracheal diameter vs lung HIF1A fold-change

Structure-function integration and correlations: Tracheal segment diameter correlated inversely with lung *HIF1A* expression ($r=-0.63$, $p=0.048$), which fits a tapering conduit and higher downstream oxygen demand. Air- capillaries density scores correlated positively with *VEGFA* ($\rho=0.71$, $p=0.021$). The link between *HIF1A* and *VEGFA* was strong ($r=0.68$, $p=0.029$). These associations held after FDR correction at $q<0.10$. The results show aligned architecture and gene programs. The exchange core shows dense capillaries and higher hypoxia-angiogenic tone. The conduit shows lower signaling and wider lumens proximally. Histology codes did not correlate with *TNF* in any field (all $p>0.20$).

Table 5. RT-qPCR performance metrics (efficiency, R², Cq of calibrator, reference gene stability)

Gene	Amplicon (bp)	Efficiency	R²	Calibrator Cq (mean ± SD)	Melt peak (°C)
HIF1A	111	0.96	0.998	27.8 ± 0.25	83.5
VEGFA	120	0.98	0.997	28.2 ± 0.28	81.9
TNF	105	0.95	0.996	30.6 ± 0.31	84.2
ACTB	142	0.99	0.999	23.9 ± 0.18	85.0
Reference stability (geNorm M)	—	—	—	0.42 (*ACTB*)	—

Gross variables did not correlate with *TNF* either. The absence of a significant difference in TNF expression between tracheal and lung tissues suggests that no marked tissue-specific increase in TNF-associated inflammatory signaling was detected under the conditions examined. Since the measurement was confined to only TNF, a lack of a wider inflammatory response cannot be ruled out. Expression and codes were symmetric for left-right lung comparisons (all $p>0.10$). Collectively these findings corroborate the notion that avian respiratory tissues are specialized for oxygen and vascular signals without background inflammation in a functionally healthy state. This in turn strengthens the biological model established from combining gross, histological and molecular layers.

Table 5. Correlations among morphometry, histology codes, and gene expression (r or ρ, 95% CI, *p*, and FDR *q*)

Variables compared	Coefficient	95% CI	p-value	FDR q
Tracheal diameter (segment mean) vs lung *HIF1A*	r = −0.63	−0.90 to −0.02	0.048	0.096
Air- capillaries density score vs lung *VEGFA*	ρ = 0.71	0.16 to 0.93	0.021	0.063
Lung *HIF1A* vs lung *VEGFA*	r = 0.68	0.07 to 0.91	0.029	0.087
Histology codes (any) vs lung *TNF*	r ≈ 0.00	—	>0.20	—
Gross variables (any) vs lung *TNF*	r ≈ 0.00	—	>0.20	—

Discussion

The trachea in the hoopoe (*Upupa epops*) appear long flexible tube is long cylindric in shape building from complete overlapping circular cartilages rings attach by annular ligaments. These results agreed in bee-eaters' birds with Al-Mamoori & Al-Ghakany (2015) and Alber et al. (2021) results. The number of cartilage rings in the hoopoe were 74.5±0.22 and its diameter decrease gradually as flows 0.33±0.001 cm, 0.28±0.02 cm, 0.21±0.004 cm toward body cavity in cranial, middle and caudal part of trachea, respectively. These findings differ from those reported in the bee-eater (Merops orientalis) by Al-Mamoori & Al-Ghakany (2015), which may reflect interspecific differences in body size and cervical anatomy. Our gross and histology results fit what modern sources report for avian airways. The trachea showed ciliated pseudostratified

columnar epithelium with goblet cells. The wall had a lamina propria, submucosa with glands, hyaline cartilage. These results were similar with Al-Ahmed and Sadoon (2020) in drack and ducking and an outer adventitia. Inside the lung show secondary bronchi which lined by ciliated columnar epithelium (pseudostratified) under lining. There is connective tissue muscle (lamina propria). Submucosa contains fibrous tissue and smooth muscle fibers. The walls of bronchioles are narrowed to small tube called parabronchi. Sections of lung contained parabronchi, atria, infundibula and dense air capillaries. That configuration supports over a period a non stop gaseous transfer and also a tight exchange core. These points are in accord with recent reviews of airway structure. (2024); de Bruin et al (2025). The trachea-scoring mucociliary phenotype is coherent with alternative, recent experimental models. The long-term chicken tracheal organoids resemble a pseudostratified epithelium containing ciliated, goblet and basal cells in vitro under air-liquid interface. The photomicrographs are similar in the cell types and sympathetic glandular support. This is consistent with our interpretation of a functional mucociliary apparatus in proximal segments and the observed decrease in gland density caudally. Collectively, these findings bolster the idea that hoopoe trachea reflects a conventional bird structure adapted for efficient conditioning and clearance (Riyaz Tramboo et al., 2024; de Bruin et al., 2025). The increased lung expression of genes associated to the hypoxia-angiogenesis coupling, such as HIF1A and VEGFA in birds. Studies in poultry show that HIF-1α activity promotes the growth of endothelium and blood vessel remodeling within the pulmonary circuit. Consistent with our findings that exchange tissue promotes increased HIF1A signal, loss of HIF-1α in broiler pulmonary artery endothelium inhibits cell growth and proliferation [12]. Hypoxic chicken cell transcriptomic work also finds large HIF-1-driven programs, and we find that the positive correlation between HIF1A and VEGFA mirrors these axes. Therefore, the molecular signature in the hoopoe lungs is biologically consistent with postulated and exhibitory echolocation biology and vascular control mechanisms atADD. (Hossain et al., 2024; Peng et al., 2024 Reheman). The low TNF signal also establish a baseline, non-inflamed state in our healthy birds. In challenge models, avian respiratory tissues experience rapid cytokine peaks including TNF, and other pro-inflammatory mediators. These rise and fall depending on the stimulus and time. This is because our samples had no such stimuli by which to elicit a response, thus explaining the flat TNF profile and lack of histologic injury. Recent analysis of respiratory cytokine storms provides some insight into the reasons for these excess amounts of cytokines causing vascular leakage and loss of endothelial barrier function. The absence of any of these signatures from our cohort lends support to confidence in the agreed structural–molecular match (Alalwany et al.,2015; Jang et al., 2013; Hossain et al., 2024; Riyaz Tramboo et al., 2024). Finally, our RT-qPCR workflow adopts the recent guidance on normalization and assay quality in birds. We validated ACTB stability vs. alternative controls and yielded efficiencies in the acceptable ranges. These steps are consistent with the currently available information for porcine reference genes and should guide characterization in specific contexts before their use. Through incorporation of these controls with blinded histology coding and defined statistics we minimize bias while validating the structure-function associations observed. Other than potentially minor primer validation this framework

should be reproducible in other small passerines or near-passerine species (Na et al., 2021; Chen et al., 2023).

Conclusions: The specialized respiratory system of birds, as represented by the hoopoe (Upupa epops) contains all the morphological and histological characteristics. The respiratory system consists of a conical trachea and an intricate pulmonary exchanging structure of barabronchi, atrium, funnel and air capillaries. The data demonstrated that lung transcript levels of HIF1A and VEGFA were higher than trachea. In the meantime, there was no marked dissimilarity between both tissues on TNF expression (data not shown). Such observations imply that pulmonary exchange tissue is linked to unique vascular signaling and corresponding responses to oxygen. The observed elevated transcript level of both HIF1A and VEGFA cannot be considered direct evidence for tissue hypoxia or ongoing angiogenesis, as complementary protein and physiological measurements were not carried out. The integrated morphological, histological and molecular approach employed here provides this study as a useful foundation for investigating respiratory specialization in the hoopoe and other avian species. Because the sex of the birds could not be determined at the time of sampling, potential sex-related differences in respiratory morphology and gene expression could not be evaluated. This should be considered a limitation of the present study and may have introduced additional biological variability into the results. The relatively small sample size is an important limitation of the present study. Although paired tissue comparisons were performed within individual birds, the small number of biological replicates limits the statistical power of correlation analyses and reduces the generalizability of the findings. Therefore, the observed associations between gene expression and morphological or histological characteristics should be considered exploratory and require confirmation in larger cohorts.

Author contribution

The author was equally responsible for study conception and design, experimental work, data collection, data analysis, and manuscript preparation.

Data availability statement

All data that support the findings are available upon reasonable request.

Acknowledgments

The authors would like to express their sincere appreciation to the staff of the Department of Anatomy and Histology, College of Veterinary Medicine, al- Qasim Green University, for their technical support and provision of laboratory facilities.

Funding

The study was self-funded by the authors and had no external source of funding.

Ethical consideration

All procedures involving animals were approved by the Ethics Committee of the College of Veterinary Medicine, Al-Qasim Green University, Babylon, Iraq (approval no. QGEC/73/2026). The study was conducted in accordance with institutional guidelines for the care and use of animals in scientific research. All efforts were made to minimize animal stress and discomfort.

Conflict of interests

The authors declare no competing interests. No financial or personal relationships influenced the work.

References

Al-Ahmed, A. S., & Sadoon, A. H. (2020). Comparative anatomical, histological and histochemical study (larynx, syrinx and trachea) between mature and immature males of local duck (*Anas platyrhynchos*). *Basrah Journal of Veterinary Research, 19*(1), 10-34. https://doi.org/10.23975/bjvetr.2021.170597

Al-Alwany, E. A. H. (2019). Association of testes histological changes with FSH and TSH hormones levels in *Fundulus heteroclitus* from the Great Bay, U.S.A. *Biochemical and Cellular Archives, 19*(Supplement 1), 2403-2407. https://connectjournals.com/pages/articledetails/toc030126

Al-Alwany, E. A. H., Al-Saadi, H. K., & Hassan, A. J. (2015). Effect of Sustanon on some immunological and hormonal parameters in rats. *International Journal of Chemical Sciences, 13*, 1947-1960. https://api.semanticscholar.org/CorpusID:55032895

Alber, A., Stevens, M. P., & Vervelde, L. (2021). The bird's immune response to avian pathogenic *Escherichia coli*. *Avian Pathology, 50*(5), 382-391. https://doi.org/10.1080/03079457.2021.1873246

Al-Khakani, S. S. A., Al-Jebori, J. G. A., & Alzubaidi, K. A. Z. (2020). Some macroscopic and morphometrical study of lower respiratory system in adult pigeons (*Streptopelia decaocto*). *Plant Archives, 20*(Supplement 1), 2792-2795. https://www.plantarchives.org/List%20SI%2020,%20SUPP-1,2020.html

Al-Khamas, A. J. H., Al-Janabi, S. M., Murtadha, O., ... & Baneen, K. A. (2024). Morphological and histological study of testis in hoopoe bird (*Upupa epops*). *Journal of Animal Health and Production, 12*(Special Issue 1), 253-257. https://api.semanticscholar.org/CorpusID:274586724

Al-Mamoori, N. A. H., & Al-Taee, N. S. N. (2020). Effects of cement dust on electrolytes and osmolality in serum and urine of Kufa Cement Factory workers. *Indian Journal of Forensic Medicine & Toxicology, 14*(3), 1605-1609. https://doi.org/10.37506/ijfmt.v14i3.10643

Al-Mamoori, N. A. M., & Al-Ghakany, S. S. A. (2015). Anatomical and morphometric study of the trachea in bee-eater bird (*Merops orientalis*). *IOSR Journal of Agriculture and Veterinary Science, 8*(10 Ver. II), 58-61. https://doi.org/10.9790/2380-081025861

Alumeri, S. K. W., Al-Abdula, M. A. A., & Al-Khakani, S. S. A. (2025). Anatomical investigation of cutaneous plantar mechanoreceptor pathways and their connections to hypothalamic structures in laboratory rats. *Open Veterinary Journal, 15*(9), 4114-4120. https://doi.org/10.5455/OVJ.2025.v15.i9.16

Boo, S. Y., Tan, S. W., Alitheen, N. B., Ho, C. L., Omar, A. R., & Yeap, S. K. (2020). Identification of reference genes in chicken intraepithelial lymphocyte natural killer cells infected with very-virulent infectious bursal disease virus. *Scientific Reports, 10*, Article 8561. https://doi.org/10.1038/s41598-020-65474-3

Chen, J., Chen, Z., Zhang, J., Zhuang, W., & Zheng, X. (2023). Screening of reliable reference genes for the normalization of RT-qPCR in chicken gastrointestinal tract. *Poultry Science, 102*(12), Article 103169. https://doi.org/10.1016/j.psj.2023.103169

de Bruin, A. C. M., Lamers, M. M., Haagmans, B. L., Leijten, L. M., Fouchier, R. A. M., & Richard, M. (2025). Long-term culture of chicken tracheal organoids for the purpose of avian influenza virus research. *Virology Journal, 22*(1), Article 99. https://doi.org/10.1186/s12985-025-02714-w

Ghazal, K. M., & Al-Alwany, E. A. H. (2025). A comparative histochemical developmental study of the kidney and ureter in golden hamster (*Mesocricetus auratus*). *Open Veterinary Journal, 15*(10), 4873-4884. https://doi.org/10.5455/OVJ.2025.v15.i10.7

Hamad, R., & Al-Alwany, E. (2024). Comparative histochemical study of pancreas in Eurasian collared dove (*Streptopelia decaocto*) and buzzard (*Buteo buteo vulpinus*). *Assiut Veterinary Medical Journal, 70*(183), 642-652. https://doi.org/10.21608/avmj.2024.303802.1303

Hossain, I., Shila, R. A., Uddin, M. M., Chowdhury, E. H., Parvin, R., & Begu, J. A. (2024). A comparative analysis of innate immune responses in Sonali and broiler chickens infected with tribasic H9N2 low pathogenic avian influenza virus. *BMC Veterinary Research, 20*, Article 500. https://doi.org/10.1186/s12917-024-04346-8

Huang, S. C., Rehman, M. U., Lan, Y. F., Qiu, G., Zhang, H., Iqbal, M. K., Luo, H. Q., Mehmood, K., Zhang, L. H., & Li, J. K. (2017). Tibial dyschondroplasia is highly associated with suppression of tibial angiogenesis through regulating the HIF-1α/VEGF/VEGFR signaling pathway in chickens. *Scientific Reports, 7*, Article 9089. https://doi.org/10.1038/s41598-017-09664-6

Jang, H., Koo, B. S., Jeon, E. O., Lee, H. R., Lee, S. M., & Mo, I. P. (2013). Altered pro-inflammatory cytokine mRNA levels in chickens infected with infectious bronchitis virus. *Poultry Science, 92*(9), 2290-2298. https://doi.org/10.3382/ps.2013-03116

Khan, A. H. A. A., Al-Alwany, E. A. H., Al-Azawi, R. S. A., Al-Jebori, J. G. A., Alkafagy, S. M., Al-Khakani, S. S. A., Al-Shukri, H. H. K., & Abdulhasan, A. S. (2025). Serum level of IL-37 as a modulator in atherosclerosis, correlating its levels with oxidative stress and disease progression. *Regulatory Mechanisms in Biosystems, 16*(2), Article e25076. https://doi.org/10.15421/0225076

König, H. E., Korbel, R., & Liebich, H.-G. (Eds.). (2016). *Avian anatomy: Textbook and colour atlas* (C. Klupiec, Trans.). 5m Publishing.

Lee, C., Kim, M. J., Kumar, A., Lee, H.-W., Yang, Y., & Kim, Y. (2025). Vascular endothelial growth factor signaling in health and disease: From molecular mechanisms to therapeutic perspectives. *Signal Transduction and Targeted Therapy, 10*, Article 170. https://doi.org/10.1038/s41392-025-02249-0

Malila, Y., Thanatsang, K., Arayamethakorn, S., Uengwetwanit, T., Srimarut, Y., Petracci, M., et al. (2019). Absolute expressions of hypoxia-inducible factor-1 alpha (HIF1A) transcript and the associated genes in chicken skeletal muscle with white striping and wooden breast myopathies. *PLoS ONE, 14*(8), Article e0220904. https://doi.org/10.1371/journal.pone.0220904

Na, W., Wang, Y., Gong, P., Zhang, X., Zhang, K., Zhang, H., Wang, N., & Li, H. (2021). Screening of reference genes for RT-qPCR in chicken adipose tissue and adipocytes. *Frontiers in Physiology, 12*, Article 676864. https://doi.org/10.3389/fphys.2021.676864

Peng, W., Fang, W., Gao, X., Guo, X., Li, G., Guo, F., Hu, G., Zhuang, Y., Li, L., Jiang, C., & Liu, P. (2024). Effect of RNA interference with HIF-1α on the growth of pulmonary artery endothelial cells in broiler chickens. *Poultry Science, 103*(5), Article 103388. https://doi.org/10.1016/j.psj.2023.103388

Reheman, A., Wu, Q., Xu, J., He, J., Qi, M., Li, K., Cao, G., & Feng, X. (2024). Transcriptomic analysis of the hypoxia-inducible factor 1 α impact on the gene expression profile of chicken fibroblasts under hypoxia. *Poultry Science, 103*(3), Article 103410. https://doi.org/10.1016/j.psj.2023.103410

Rhodes, E. M., Yap, K. N., Mesquita, P. H. C., Parry, H. A., Kavazis, A. N., Krause, J. S., Hill, G. E., & Hood, W. R. (2024). Flexibility underlies differences in mitochondrial respiratory performance between migratory and non-migratory White-crowned Sparrows (*Zonotrichia leucophrys*). *Scientific Reports, 14*, Article 9456. https://doi.org/10.1038/s41598-024-59715-y

Tramboo, S. R., Elkhalifa, A. M. E., Quibtiya, S., Ali, S. I., Nazir Shah, N., Taifa, S., Rakhshan, R., Hussain Shah, I., Ahmad Mir, M., Malik, M., Ramzan, Z., Bashir, N., Ahad, S., Khursheed, I., Bazie, E. A., Mohamed Ahmed, E., Elderdery, A. Y., Alenazy, F. O., Alanazi, A., Alzahrani, B., ... & Nabi, S. U. (2024). The critical impacts of cytokine storms in respiratory disorders. *Heliyon, 10*(9), Article e29769. https://doi.org/10.1016/j.heliyon.2024.e29769

Wang, D., Zhang, Q., Zhang, Z., Zhang, Y., Wang, S., Han, Y., Zhu, H., & He, H. (2024). Expression profile of Toll-like receptors and cytokines in the cecal tonsil of chickens challenged with *Eimeria tenella*. *Parasitology Research, 123*, Article 347. https://doi.org/10.1007/s00436-024-08371-2

Zhang, X., Yang, Y., & Shi, Q. (2025). DNA methylation in adaptation to high-altitude environments and pathogenesis of related diseases. *Human Genomics, 19*, Article 100. https://doi.org/10.1186/s40246-025-00794-x

مجله بیوتکنولوژی کشاورزی
شاپا چاپی: ۶۷۰۵-۲۲۲۸ شاپا الکترونیکی: ۶۵۰۰-۲۲۲۸

بررسی ریخت‌شناختی، بافت‌شناختی و الگوی بیان ژن در دستگاه تنفسی هدهد عراقی (*Upupa epops*)

سلیم صالح علی الخاقانی
گروه آناتومی و بافت‌شناسی، دانشکده دامپزشکی، دانشگاه القاسم الخضراء، بابل، ۵۱۰۱۳، عراق. ایمیل: salimsalih@vet.uoqasim.edu.iq
رنین صفاء حمد
گروه آناتومی و بافت‌شناسی، دانشکده دامپزشکی، دانشگاه القاسم الخضراء، بابل، ۵۱۰۱۳، عراق. ایمیل: ranin@vet.uoqasim.edu.iq
علی کاظم حمادی الجبوری
گروه تولیدات دامی، دانشگاه سومر، دانشکده کشاورزی، بابل، ۵۱۰۱۳، عراق. ایمیل: Alikadhem1@uos.edu.iq
اخلاص عبد حمزه العلوانی
* نویسنده مسئول. گروه آناتومی و بافت‌شناسی، دانشکده دامپزشکی، دانشگاه القاسم الخضراء، بابل، ۵۱۰۱۳، عراق. ایمیل: ekhlas.alalwany1@vet.uoqasim.edu.iq
جعفر غازی عباس الجبوری
گروه آناتومی و بافت‌شناسی، دانشکده دامپزشکی، دانشگاه القاسم الخضراء، بابل، ۵۱۰۱۳، عراق. ایمیل: jafar1@vet.uoqasim.edu.iq
مصطفی فاضل
گروه آناتومی و بافت‌شناسی، دانشکده دامپزشکی، دانشگاه القاسم الخضراء، بابل، ۵۱۰۱۳، عراق. ایمیل: mustafafadhil1@vet.uoqasim.edu.iq
احلام ج. ح. الخماس
گروه آناتومی و بافت‌شناسی، دانشکده دامپزشکی، دانشگاه القاسم الخضراء، بابل، ۵۱۰۱۳، عراق. ایمیل: ahlamalkhamas1@vet.uoqasim.ed.iq
اسامه م. کاظم
گروه آناتومی و بافت‌شناسی، دانشکده دامپزشکی، دانشگاه القاسم الخضراء، بابل، ۵۱۰۱۳، عراق. ایمیل: Osamamkadhim1@vet.uoqasim.edu.iq
آمنه عماد جواد
گروه آناتومی و بافت‌شناسی، دانشکده دامپزشکی، دانشگاه القاسم الخضراء، بابل، ۵۱۰۱۳، عراق. ایمیل: amna.imad.jawad1@vet.uoqasim.edu.iq
محمد صلاح حسن سماوی
گروه آناتومی و بافت‌شناسی، دانشکده دامپزشکی، دانشگاه القاسم الخضراء، بابل، ۵۱۰۱۳، عراق. ایمیل: mohammedsalah1@vet.uoqasim.edu.iq
سراج م. الکفاجی
گروه آناتومی و بافت‌شناسی، دانشکده دامپزشکی، دانشگاه القاسم الخضراء، بابل، ۵۱۰۱۳، عراق. ایمیل: drsirajmoner1@vet.uoqasim.edu.iq
صابرین م. الجنابی
گروه آناتومی و بافت‌شناسی، دانشکده دامپزشکی، دانشگاه القاسم الخضراء، بابل، ۵۱۰۱۳، عراق. ایمیل: Sabreen.mizher1@vet.uoqasim.edu.iq
حوراء ک. جودی
گروه فیزیک پزشکی، دانشکده دانشگاه حله، بابل، عراق. ایمیل: hawraakareemjudi1@gmail.com

تاریخ دریافت: ۱۴۰۵/۰۲/۳۱ تاریخ دریافت فایل اصلاح شده نهایی: ۱۴۰۵/۰۵/۰۵ تاریخ پذیرش: ۱۴۰۵/۰۵/۰۶

چکیده

هدف: مطالعات نشان داده‌اند که سازمان‌یافتگی آناتومیکی و عملکردی دستگاه تنفسی پرندگان بسیار تخصص‌یافته است. بااین‌حال، در هدهد (*Upupa epops*)، ویژگی‌های یکپارچه ریخت‌شناختی، بافت‌شناختی و مولکولی دستگاه تنفسی هنوز به‌طور کامل و روشن

مورد مطالعه قرار نگرفته‌اند. هدف این مطالعه، بررسی ویژگی‌های دستگاه تنفسی ه هدهد (*Upupa epops*) با استفاده از یک رویکرد یکپارچه ریخت‌شناختی، بافت‌شناختی و مولکولی بود. تجزیه‌وتحلیل مولکولی بر ژن‌های دخیل در حس‌کردن اکسیژن، پیام‌رسانی عروقی و التهاب متمرکز بود.

مواد و روش‌ها: برای مطالعه هشت هدهد بالغ (*Upupa epops*) از مورفومتری ماکروسکوپی، تجزیه‌وتحلیل بافت‌شناختی با استفاده از رنگ‌آمیزی هماتوکسیلین و ائوزین و تری‌کروم ماسون، و واکنش زنجیره‌ای پلیمراز کمی با رونویسی معکوس-RT) (qPCRاستفاده شد. تجزیه‌وتحلیل بیان ژن برای فاکتور القاشونده با هیپوکسی ۱-آلفا (HIF1A)، فاکتور رشد اندوتلیال عروقی A (VEGFA)و فاکتور نکروز توموری (TNF) انجام شد. ژن مرجع ACTB بود. برای ارزیابی اندازه‌گیری‌های مورفومتریک و سطوح بیان ژن، از آزمون‌های آماری زوجی مناسب استفاده شد. تجزیه‌وتحلیل‌های همبستگی برای بررسی ارتباط میان متغیرهای مولکولی و ساختاری به کار رفتند.

نتایج: قطر نای از قسمت جمجمه‌ای به سمت قسمت دمی به‌طور معنی‌داری کاهش یافت و این اثر از شدت بالایی برخوردار بود ($p<0.001$). ضخامت ریه چپ و راست مشابه بود ($p>0.05$). بررسی بافت‌شناختی، وجود اپی‌تلیوم مژک‌دار کاذب‌چندلایه و سلول‌های جامی را در نای نشان داد. لایه زیرمخاطی حاوی غدد سروموکوسی بود و توسط غضروف هیالین حمایت می‌شد. ریه‌ها دارای پارابرونش‌ها، دهلیزها، اینفاندیبولا و شبکه متراکمی از مویرگ‌های هوایی بودند. سطوح فاکتور القاشونده با هیپوکسی ۱-آلفا در ریه در مقایسه با نای بالاتر بود ($p<0.05$; fold-change >1.5). سطوح فاکتور رشد اندوتلیال عروقی A نیز در ریه افزایش یافت ($p<0.05$; fold-change >1.5). سطوح فاکتور نکروز توموری (TNF) پایین باقی ماندند و تفاوتی بین بافت‌ها نشان ندادند ($p>0.05$). سطوح HIF1Aو VEGFAدر نمونه‌ها همبستگی مثبت داشتند ($r>0.6, p<0.05$). بیان بتا اکتین اسکلت سلولی (ACTB) در بافت‌های مورد بررسی پایدار بود. این یافته‌های مولکولی با شبکه متراکم مویرگی مشاهده‌شده در بررسی بافت‌شناختی مطابقت داشتند.

نتیجه‌گیری: فراوانی بیشتر رونوشت HIF1A مشاهده‌شده در بافت ریه ممکن است نشان‌دهنده فعال‌شدن بیشتر مسیرهای پاسخ‌دهنده به اکسیژن باشد. بااین‌حال، از آنجا که سطوح پروتئین HIF-1α و اکسیژن‌رسانی مستقیم بافت اندازه‌گیری نشدند، این یافته‌ها نباید به‌عنوان شواهد مستقیم هیپوکسی بافتی تفسیر شوند. این رویکرد چندسطحی، استفاده از ترکیب تجزیه‌وتحلیل‌های مورفو-بافت‌شناختی و RT-qPCR را برای بررسی سلامت و سازگاری دستگاه تنفسی پرندگان تأیید می‌کند.

کلمات کلیدی: ریه، مویرگ‌های هوایی، نای، هدهد، RT-qPCR

نوع مقاله: پژوهشی

استناد: سلیم صالح علی الخاقانی، رنین صفاء حمد، علی کاظم حمادی الجبوری، اخلاص عبد حمزه العلوانی، جعفر غازی عباس الجبوری، مصطفی فاضل، احلام ج. ح. الخماس، اسامه م. کاظم، آمنه عماد جواد، محمد صلاح حسن سماوی، سراج م. الکفاجی، صابرین م. الجنابی، حوراء ک. جودی (۱۴۰۵). بررسی ریخت‌شناختی، بافت‌شناختی و الگوی بیان ژن در دستگاه تنفسی هدهد عراقی (*Upupa epops*). *مجله بیوتکنولوژی کشاورزی*، ۱۸(۴)، ۵۹۳-۶۱۴.

Publisher: Shahid Bahonar University of Kerman & Iranian Biotechnology Society.

© the authors